Multireference Configuration Interaction Calculation of the $\tilde{B}^2A''-\tilde{X}^2A''$ Transition of Halogen- and Methyl-Substituted Vinoxy Radicals

Makoto Yamaguchi,*,† Satoshi Inomata,‡ and Nobuaki Washida§

Institute of Research and Innovation, 1201 Takada, Kashiwa, Chiba, 277-0861 Japan, Division of Atmospheric Environment, The National Institute for Environmental Studies, 16-2 Onogawa, Tsukuba, Ibaraki, 305-8506 Japan, and Chemical Dynamics Laboratory, RIKEN, 2-1 Hirosawa, Wako, Saitama, 351-0198 Japan

Received: July 27, 2006; In Final Form: August 25, 2006

Ground and second excited electronic states of halogen and monomethyl substituted vinoxy radicals were studied by multireference configuration interaction (MRCI) calculation. Optimized geometries, rotational constants and vibrational frequencies of vinoxy and 1-fluorovinoxy showed good agreement with experimental values. Differences in calculated and observed $\tilde{B}-\tilde{X}$ electronic transition energies were less than 0.1 eV and observed trends of blue shift upon increasing the number of substituted halogen atoms were reproduced by MRCI calculation. Observed fluorescence lifetimes of the vibrationless level in $\tilde{B}$ state were in good agreement with calculated values. Rotational profiles of the 0−0 vibronic bands were successfully simulated with calculated rotational constants and transition dipole moments. Energy differences between planar and nonplanar optimized geometries in $\tilde{B}$ state showed good correlation with the onset of fast nonradiative decay in $\tilde{B}$ state, supporting the proposed mechanism of nonradiative decay via avoided crossings from $\tilde{B}$ to $\tilde{A}$ state which is followed by the decay to the ground state via conical intersections.

Introduction

Vinoxy radical (CH_2CHO) has received much attention in recent years as an intermediate of oxidation reactions of hydrocarbons in combustion processes.[1] Its vibronic bands in the $\tilde{B}^2A''-\tilde{X}^2A''$ transition have been experimentally studied by various methods such as electronic absorption,[2,3] laser induced fluorescence,[4−9] and photofragmentation.[10] Electronic states relevant to the transition have been characterized by ab initio MCSCF calculations.[11,12] One of the unique features of the $\tilde{B}^2A''-\tilde{X}^2A''$ transition is abrupt disappearance of the fluorescence around 1300 cm^{-1} above the 0−0 band, although vibronic levels above this threshold have been detected.[6,10] One of the authors pointed out that potential energy curves of $\tilde{A}$, $\tilde{B}$, and $\tilde{C}$ states become closer as the radical is twisted around the C−C bond and the nonradiative decay from the $\tilde{B}$ to $\tilde{A}$ state would be induced.[13] Brock et al. measured fluorescence lifetimes from single vibronic levels (SVLs) in the $\tilde{B}$ state and confirmed that the fluorescence decay rates from SVLs of out-of-plane modes are much faster than those of in-plane modes of almost equal excitation energies.[8] Nagai et al. concluded that the decay is not mediated by spin−orbit coupling, as fluorescence lifetimes from single rovibronic levels do not depend on the *K* numbers.[9]

Recently, Matsika et al. studied the nonradiative decay process of vinoxy by MRCI calculation.[14] Optimized geometries of stationary points in the $\tilde{B}$ state were calculated and nonplanar optimized geometries were 1457 cm^{-1} higher than the planar spectroscopic minimum, which was in good agreement with the observed onset of fast nonradiative decay. They also calculated potential energy curves of $\tilde{X}$, $\tilde{A}$ and $\tilde{B}$ states along the C−C torsion and the CCO bend angle coordinates. Conical intersections between $\tilde{A}$ and $\tilde{B}$ states were found to be much higher in energies and not relevant to the fast nonradiative decay. They estimated nonradiative decay rates from vibrational levels in the $\tilde{B}$ state by assuming one-dimensional potential energy curves along the reaction coordinate and using nonadiabatic coupling vectors between $\tilde{A}$ and $\tilde{B}$ states by MRCI calculation. The relaxation rate becomes much faster when the vibrational wave function is delocalized between planar and nonplanar local minima and they concluded that the decay from the $\tilde{B}$ to $\tilde{A}$ state is not mediated by the conical intersection but nonadiabatic coupling.

Although it is not so extensive as in the case of unsubstituted vinoxy, spectroscopic properties and reactions of halogen[15−20] and methyl[21−25] substituted vinoxy radicals have been studied in recent years mainly by laser induced florescence spectra of the $\tilde{B}-\tilde{X}$ transition. Transition energies, fluorescence lifetimes, vibronic structures, rotational profiles, and onset of the fast decay were dependent on chemical structures and positions of substituents. We have already shown in the case of unsubstituted and halogenated vinoxy radicals that CASSCF calculation provides excitation energies and vibrational frequencies that are helpful for assignment of vibronic peaks in fluorescence spectra.[18−20] However, discrepancies between calculated and observed excitation energies exceeded 0.1 eV in some cases and observed blue shift of excitation energies by increasing the number of substituted atoms were not correctly reproduced.[26] These results imply that dynamical correlation must be taken into account to obtain quantitatively accurate potential energy surfaces of the excited states.[23,24] In this paper results of MRCI calculation of vinoxy type radicals are presented that successfully reproduced spectroscopic properties of these radicals and implication to nonradiative decay mechanism of vinoxy type radicals will be discussed.

* Corresponding author. E-mail: m-ymgc@iri.or.jp.
† Institute of Research and Innovation.
‡ The National Institute for Environmental Studies.
§ RIKEN.

10.1021/jp0647840 CCC: $33.50
Published on Web 10/26/2006

TABLE 1: Planar Optimized Geometries and Rotational Constants of CH_2CHO

		geometrical parameters			rotational constants		
state	method and basis sets	r(C_1-C_2) (Å)	r(C_2-O) (Å)	∠(C_1C_2O) (deg.)	A (cm^{-1})	B (cm^{-1})	C (cm^{-1})
$\tilde{X}(^2A'')$	MRCISD/cc-pVDZ[a]	1.437	1.236	122.8	2.2166	0.3784	0.3232
	MRCISD/DZP+[b]	1.445	1.238	122.5	2.2109	0.3771	0.3221
	QCISD/6-31G**[c]	1.434	1.241	122.6	2.2202	0.3790	0.3237
	RCCSD(T)/cc-pCVQZ[d]	1.429	1.226	122.9	2.2503	0.3837	0.3278
	Experiment[e]	1.405	1.272	121.9	2.228	0.3809	0.3253
	Experiment[f]	1.408	1.261	122.4	2.2241	0.3818	0.3255
$\tilde{B}(^2A'')$	MRCISD/cc-pVDZ[a]	1.447	1.374	122.7	2.0772	0.3429	0.2943
	MRCISD/DZP+[b]	1.452	1.376	121.6	2.0488	0.3452	0.2954
	EOMEE-CCSD/cc-pVDZ[g]	1.434	1.378	123.1	2.090	0.343	0.295
	Experiment[e]	1.466	1.337	129.5	2.103	0.3442	0.2958
		(1.43[h])	(1.38[h])	(123.1[h])			
	Experiment[i]				2.1090	0.3434	0.2989

[a] This work. [b] Reference 14. [c] Reference 10. [d] Reference 50. [e] Reference 5. [f] Reference 52. [g] Reference 23. [h] Recalculation by Williams *et al.*[23] [i] Reference 8.

Computational Method

The latest release of the COLUMBUS program[27−30] was used for MRCI calculations because the program is capable of geometry optimization with analytical gradients calculated at the MRCI level[31−34] and the method has been successfully applied to calculation of potential energy curves of valence and Rydberg excited states of polyatomic molecules.[35,36] Dunning's cc-pVDZ type basis sets were used for all the molecules in this study.[37,38] State averaged complete active space self-consistent field (SA-CASSCF) calculations were performed by averaging the ground ($\tilde{X}$) and the lowest three excited states ($\tilde{A}$, $\tilde{B}$, $\tilde{C}$) with equal weighting factors. Twenty configuration state functions (CSFs) were generated by five electrons in four molecular orbitals (one a′ and three a″ molecular orbitals at Cs symmetry). In MRCI calculation CSFs were generated by single and double excitation from the reference space (denoted as MRCISD) and the 1s orbital of C, O, F atoms and 1s, 2s, and 2p orbitals of Cl were chosen as frozen cores. Numbers of generated configurations were 1−10 million with generalized interaction restriction. Geometry optimization was performed with the GDIIS method[39] until maximum and root mean square (rms) changes of coordinates and forces became less than 10^{-3}. Hessians were numerically calculated by using analytical gradients at geometries slightly deformed from the optimized geometry along natural internal coordinates.[40,41] State energies after Davidson's correction were calculated and those values were denoted as MRCISD+Q.[42,43] Transition moments between $\tilde{X}$ and $\tilde{B}$ states were calculated by using molecular orbitals obtained from SA-CASSCF calculation at the planar optimized geometries in the $\tilde{B}$ state. CASSCF calculations were performed by using the Gaussian03 program[44] with 6-31G* basis sets[45−48] and complete active space generated from seven electrons in five molecular orbitals. Rotational profiles of the 0−0 bands were simulated with the SPECVIEW program.[49] Molecules were assumed as asymmetric tops, and spin rotation was not taken into account. Rotational constants of planar optimized geometries in $\tilde{X}$ and $\tilde{B}$ states by MRCISD calculation were calculated with the Gaussian03 program.

Optimized Geometries, Rotational Constants, and Vibrational Frequencies of CH_2CHO and CH_2CFO. First we summarize results of MRCISD calculation for CH_2CHO and CH_2CFO because these radicals have been extensively studied both experimentally and theoretically and the results of the present MRCISD calculation can be critically examined. The molecular structure of vinoxy type radicals is shown in Figure 1. Geometrical parameters and rotational constants of planar optimized geometries of the CH_2CHO radical in the ground $\tilde{X}^2A''$ and the second excited $\tilde{B}^2A''$ states are summarized in Table 1. The optimized geometry of CH_2CHO in the ground $\tilde{X}^2A''$ state by MRCISD calculation is very close to those reported in recent literature summarized by Botschwina.[50] As for the experimentally determined geometry, DiMauro et al. calculated CC and CO bond lengths from rotational constants determined from supersonic jet LIF spectra.[5] Other geometrical parameters were fixed to calculated values by Dupuis et al.,[11] which were the most reliable at the time of their study. Endo et al. determined CC and CO bond lengths and CCO bond angles by using rotational constants of CH_2CHO[51] and CD_2CDO[52] derived from microwave spectra. They adjusted CH bond lengths 0.01 Å longer to get better agreement with the calculated and measured rotational constants. However, the method and basis sets employed for the calculation by Dupuis et al. may not give very accurate values as recent calculations. Experimental values show much shorter CC bond lengths and longer CO bond lengths than calculated values, although the sum of CC and CO bond lengths are very close to those of optimized geometries.

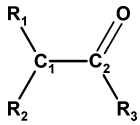

Figure 1. Molecular structure of vinoxy type radical.

As for the excited $\tilde{B}^2A''$ state, optimized geometries reported by Williams et al.[23] and Matsika et al.[14] were very close to the result of the present calculation. DiMauro et al. derived the CO bond length and the CCO bond angle by the same procedure as in the case of the ground state.[5] However, the CCO angle was too large judging from the absence of long progression of CCO bending modes in fluorescence spectra, as expected from the large change of the CCO bond angle by the $\tilde{B}-\tilde{X}$ transition. Williams et al. derived geometrical parameters that reproduce measured rotational constants by using their optimized geometry as an initial guess.[23] Only slight modification was necessary to obtain final values, indicating that calculated geometries were very close to the actual equilibrium geometry in the $\tilde{B}$ state.

Table 2 summarizes optimized geometries and rotational constants of CH_2CFO radical. The optimized geometry of the ground $\tilde{X}^2A''$ state by MRCISD calculation shows good agreement with recently reported optimized geometries by Cao et al.[53] and Hoops et al.[25] Calculated rotational constants from optimized geometries showed that the molecule is close to an oblate top, in contrast to the case of CH_2CHO as a prolate top. Wright et al. analyzed rotational band profiles in fluorescence excitation spectra and determined rotational constants as listed in the table, which are in good agreement with calculated values.[17] As for the excited state, the planar optimized geometry

TABLE 2: Planar Optimized Geometries and Rotational Constants of CH_2CFO

		geometrical parameters			rotational constants		
state	method and basis sets	$R(C_1-C_2)$ (Å)	$R(C_2-O)$ (Å)	$\angle(C_1C_2O)$ (deg)	A (cm^{-1})	B (cm^{-1})	C (cm^{-1})
$\tilde{X}(^2A'')$	MRCISD/cc-pVDZ[a]	1.441	1.199	126.6	0.3841	0.3581	0.1853
	B3LYP/6-311G** [b]	1.436	1.196	127.3	0.3793	0.3587	0.1843
	QCISD/6-311G** [c]	1.451	1.196	127.2	0.3797	0.3583	0.1844
	experiment[d]				0.3603		0.1846
$\tilde{B}(^2A'')$	MRCISD/cc-pVDZ[a]	1.416	1.348	129.1	0.3782	0.3360	0.1779
	experiment[d]				0.3452		0.1806

[a] This work. [b] Reference 53. [c] Reference 25. [d] Reference 17.

TABLE 3: Vibrational Frequencies of CH_2CHO (cm^{-1})

	$\tilde{X}(^2A'')$			$\tilde{B}(^2A'')$	
	MRCISD/cc-pVDZ[a]	QCISD/6-31G** [b]	exp	MRCISD/cc-pVDZ[a]	exp[d]
$C_1H_1H_2$ asym str	3215	3198	not observed	3230	not observed
$C_1H_1H_2$ sym str	3097	3084	not observed	3116	not observed
C_2H_3 str	2949	2916	2828[c]	3092	not observed
C_2O str.	1523	1519	1543[d]	1724	1621
$C_1H_1H_2$ scis	1441	1452	1486[d]	1398	1405
OC_2H_3 bend	1367	1373	1366[d]	1289	1274
$C_1H_1H_2$ rock	1125	1125	1143[d]	1116	1122
C_1C_2 str	951	947	957[d]	913	917
C_1C_2O bend	486	484	500[d]	434	449
C_2OH_3 wag	943	932	703[d]	631	595
$C_1H_1H_2$ wag	677	680	557[d]	488	436
C_1C_2 torsion	423	425	404[d]	376	274

[a] This work. [b] Reference 18. [c] Reference 55. [d] Reference 8.

TABLE 4: Vibrational Frequencies of CH_2CFO (Units in cm^{-1})

	$\tilde{X}(^2A'')$			$\tilde{B}(^2A'')$	
	MRCISD/cc-pVDZ[a]	QCISD/6-311G** [b]	exp[b]	MRCISD/cc-pVDZ	exp[b]
$C_1H_1H_2$ asym. str.	3268	3172	not observed	3275	not observed
$C_1H_1H_2$ sym. str.	3141	3052	not observed	3157	not observed
C_2O str.	1717	1715	1724	1877	1790
$C_1H_1H_2$ scis.	1441	1415	1475	1423	1409
C_2F str.	1268	1215	1211	1351	1253
$C_1H_1H_2$ rock	1001	980	906	970	911
C_1C_2 str,	884	851	847	877	874
C_1C_2F bend	600	585	584	536	537
C_1C_2O bend	411	408	416	403	421
C_2OF wag	729	698	not observed	641	not observed
$C_1H_1H_2$ wag	598	577	not observed	508	not observed
C_1C_2 torsion	324	307	not observed	474	not observed

[a] This work. [b] Reference 25.

shows not only elongation of CO but also changes in CC bond length and CCO angle, in contrast to the case of CH_2CHO. All the calculated rotational constants of the excited state are smaller than those of the ground state that is consistent with the changes of experimentally determined rotational constants.

Tables 3 and 4 show experimental and calculated vibrational frequencies at planar optimized geometries in $\tilde{X}$ and $\tilde{B}$ states of CH_2CHO and CH_2CFO radicals, respectively. All the values are positive, indicating the planar optimized geometries of these radicals are real local minima on the potential energy surfaces. Calculated vibrational frequencies in previous literature are cited in the table, and values are scaled by 0.9538, as proposed by Radom et al. for QCISD/6-31G(d) calculation.[54] Vibrational frequencies in the ground state by MRCISD calculation in this study and QCISD calculations by Hoops et al. are very close in all the vibrational modes and they show good agreement with experimental values for in-plane modes but agreement is less satisfactory for out-of-plane modes. Calculated vibrational frequencies show very good agreement with experimental values also in the excited state except for CO and CF (for CH_2CFO only) stretching modes.

Optimized Geometries of Other Vinoxy Type Radicals. No experimental values of geometrical parameters and rotational constants are available for other vinoxy type radicals. Table 5 summarizes optimized geometries and calculated rotational constants of vinoxy type radicals. Only CC and CO bond lengths and CCO bond angles are listed in the table, and all the geometrical parameters are summarized in Tables S1−S12 as Supporting Information. Figure 2 shows plots of CO bond lengths against CC bond lengths to observe the substituents' effect on the CCO structure of vinoxy type radicals. Plotted points form two groups with longer (>1.2 Å) and shorter (<1.2 Å) CO bond lengths, whereas the average CC bond lengths of those two groups are almost the same in the ground state. The group with longer CO bonds includes CHXCHO (X = H, Cl, CH_3) radicals and CH_2COCH_3, whereas 1-halogenated radicals have shorter CO bonds. The substituent effect on CO bond lengths is similar to the case of acetyl compounds: Experimental values of CO bond lengths of acetyl fluoride (1.181 Å) and acetyl chloride (1.187 Å) are shorter than those of acetaldehyde (1.216 Å) and acetone (1.215 Å).[56] In the case of the $\tilde{B}$ state, plotted points in Figure 3 form two groups with the same

TABLE 5: Planar Optimized Geometries and Rotational Constants of Vinoxy Type Radicals

		geometrical parameters			rotational constants		
species	state	$R(C_1-C_2)$ (Å)	$R(C_2-O)$ (Å)	$\angle(C_1C_2O)$ (deg)	A (cm^{-1})	B (cm^{-1})	C (cm^{-1})
CH_2ClO	$\tilde{X}(^2A'')$	1.444	1.204	125.4	0.3776	0.1692	0.1169
	$\tilde{B}(^2A'')$	1.424	1.352	126.5	0.3429	0.1770	0.1167
CH_2COCH_3	$\tilde{X}(^2A'')$	1.449	1.234	120.2	0.3639	0.3010	0.1700
	$\tilde{B}(^2A'')$	1.444	1.374	121.6	0.3349	0.2986	0.1626
trans-CHClCHO	$\tilde{X}(^2A'')$	1.440	1.229	121.3	1.6997	0.0893	0.0848
	$\tilde{B}(^2A'')$	1.442	1.370	120.8	1.6397	0.0854	0.0812
cis-CHClCHO	$\tilde{X}(^2A'')$	1.443	1.227	124.3	0.6104	0.1271	0.1052
	$\tilde{B}(^2A'')$	1.442	1.367	123.5	0.5428	0.1265	0.1026
trans-CH_3CHCHO	$\tilde{X}(^2A'')$	1.435	1.235	123.2	1.4097	0.1380	0.1287
	$\tilde{B}(^2A'')$	1.448	1.371	122.6	1.3616	0.1304	0.1217
cis-CH_3CHCHO	$\tilde{X}(^2A'')$	1.438	1.235	123.4	0.6474	0.1937	0.1534
	$\tilde{B}(^2A'')$	1.442	1.377	121.7	0.5764	0.1946	0.1495
trans-CHFCFO	$\tilde{X}(^2A'')$	1.440	1.193	127.2	0.3782	0.1318	0.0977
	$\tilde{B}(^2A'')$	1.413	1.346	128.6	0.3533	0.1292	0.0946
cis-CHFCFO	$\tilde{X}(^2A'')$	1.437	1.197	124.3	0.3644	0.1407	0.1015
	$\tilde{B}(^2A'')$	1.418	1.347	126.6	0.3687	0.1318	0.0971
cis-CHClCFO	$\tilde{X}(^2A'')$	1.447	1.197	123.9	0.3610	0.0822	0.0669
	$\tilde{B}(^2A'')$	1.409	1.346	129.0	0.3667	0.0785	0.0647
trans-CHClCFO	$\tilde{X}(^2A'')$	1.450	1.192	127.8	0.3775	0.0771	0.0640
	$\tilde{B}(^2A'')$	1.417	1.348	126.2	0.3538	0.0769	0.0632

TABLE 6: Observed and Calculated Transition Energies of the $\tilde{B}-\tilde{X}$ Transition

		calculated (cm^{-1})	
	observed (cm^{-1})	CAS(7,5)/6-31G*	MRCISD+Q/cc-pVDZ
CH_2CHO	28784[a]	28571	29008
CH_2CFO	29867[b]	31013	30380
CH_2CClO	*c*	28996	28987
CH_2COCH_3	27283[d]	28660	28242
trans-CHClCHO	29040[e]	28177	29300
cis-CHClCHO	28412[e]	27951	28995
trans-CH_3CHCHO	29363[f]	29026	29570
cis-CH_3CHCHO	29090[f]	28673	29543
trans-CHFCFO	31270[g]	31131	31892
cis-CHFCFO	31644[g]	31315	32214
cis-CHClCFO	30715[g]	30883	31137
trans-CHClCFO	30066[g]	30762	30669

[a] Reference 8. [b] Reference 17. [c] Not observed. [d] Reference 23. [e] Reference 19. [f] Reference 24. [g] Reference 20.

members as in the case of the ground state. In both groups CO bonds are elongated upon excitation. However, although CC bonds are slightly elongated in CHXCHO radicals, they become shorter in 1-halogenated radicals after excitation to the $\tilde{B}$ state.

Excitation Energies. Table 6 shows measured T_0 values and calculated T_e values of the $\tilde{B}-\tilde{X}$ transition of vinoxy type radicals. Transition energies were calculated as differences of the total energies by the MRCISD+Q method, i.e., with Davidson's correction at optimized geometries of the ground and the excited states, respectively. We did not calculate T_0 values because it would be very time-consuming to estimate zero point vibration energies in $\tilde{X}$ and $\tilde{B}$ states from vibrational analyses at the MRCISD level with numerically calculated force constant matrixes. Results of CASSCF calculation were also listed for comparison. Measured values are plotted against calculated values in Figure 3. Although CASSCF calculated excitation energies showed very good agreement with the observed values in the case of CH_2CHO, there are several cases in which discrepancies between calculated and observed values exceeded 1000 cm^{-1}. On the other hand, MRCISD+Q calculated transition energies were 200−700 cm^{-1} higher than the experimental values except for CH_2COCH_3 with a larger difference (959 cm^{-1}). However, data points of the MRCISD+Q calculation plotted in Figure 3 are much less scattered than those of the CASSCF calculation and least-squares fitting of data with MRCISD+Q calculation results in the relation between T_e and

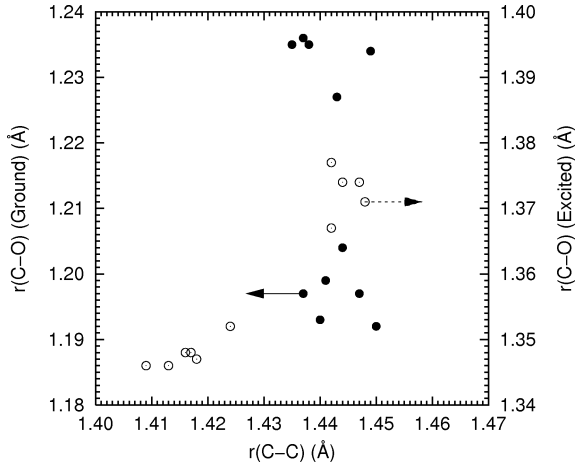

Figure 2. C−O bond lengths of planar optimized geometries in $\tilde{X}$ (filled, left scale) and $\tilde{X}$ (open, right scale) states plotted against C−C bond lengths.

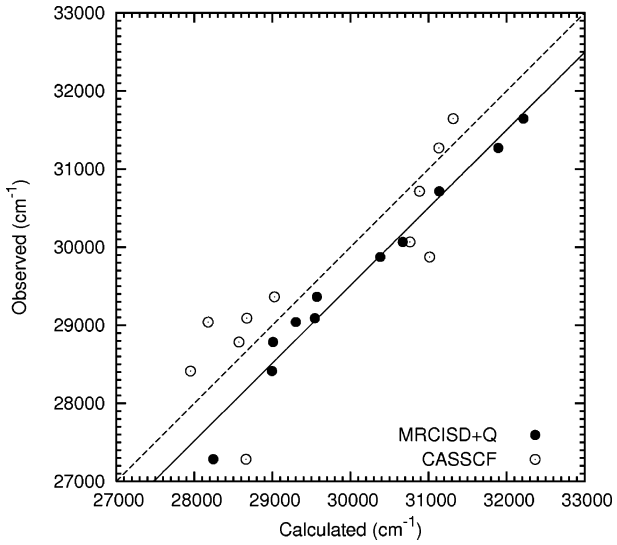

Figure 3. Observed T_0 values of the $\tilde{B}-\tilde{X}$ transition of vinoxy type radicals plotted against calculated T_e values: (solid) MRCISD+Q; (open) CASSCF. The straight line is $y = 0.995x - 352.7$ ($R^2 = 0.97$) after linear regression analysis of results of MRCISD+Q calculation, and the dotted line is $y = x$.

TABLE 7: Calculated Transition Moments and Radiative Lifetimes of the Vibrationless Level of the $\tilde{B}$ State

	transition moment (e*Bohr)		radiative lifetime (ns)	
	magnitude	b/a ratio	calc	exp
CH_2CHO	0.318	0.442	205	190[a]
CH_2CFO	0.525	0.596	67	81[b]
CH_2COCH_3	0.397	9.97	154	130[c]
trans-CHClCHO	0.369	0.279	148	135[d]
cis-CHClCHO	0.309	1.12	225	199[d]
trans-CH_3CHCHO	0.309	0.374	204	181[c]
cis-CH_3CHCHO	0.314	1.92	203	191[c]
trans-CHFCFO	0.462	2.41	76	91[e]
cis-CHFCFO	0.498	0.381	63	57[e]
cis-CHClCFO	0.603	0.223	45	25[e]

[a] Reference 8. [b] Reference 17. [c] Reference 21. [d] Reference 19. [e] Reference 20.

T_0 as T_e(calculated) = $0.995T_0$(measured) − 352.7 in cm^{-1} with a high correlation factor (R^2 = 0.97).

It should be noted that the MRCISD+Q calculation reproduced the order of measured transition energies. For example, observed T_0 values shifted toward higher energies as the number of fluorine atoms increased (CH_2CHO (28784 cm^{-1}) < CH_2CFO (29867 cm^{-1}) < *trans*-CHFCFO (31270 cm^{-1}) < *cis*-CHFCFO (31644 cm^{-1})) and the MRCISD+Q calculation could reproduce this order (CH_2CHO (29008 cm^{-1}) < CH_2CFO (30380 cm^{-1}) < *trans*-CHFCFO (31892 cm^{-1}) < *cis*-CHFCFO (32214 cm^{-1})). Another series of blue shift by fluorine atom substitution was observed experimentally for 2-chlorovinoxy radicals (*cis*-CHClCHO (28412 cm^{-1}) < *trans*-CHClCHO (29040 cm^{-1}) < *trans*-CHClCFO (30066 cm^{-1}) < *cis*-CHClCFO (30715 cm^{-1})). The MRCISD calculation was successful in reproducing this order (*cis*-CHClCHO (28995 cm^{-1}) < *trans*-CHClCHO (29300 cm^{-1}) < *trans*-CHClCFO (30669 cm^{-1}) < *cis*-CHClCFO (31137 cm^{-1})). On the other hand, the CASSCF calculation did not reproduce this correct order.

Transition Moments and Radiative Lifetimes. Table 7 shows transition dipole moments by MRCISD calculation at planar optimized geometries in the $\tilde{B}$ state. Not only magnitudes but also ratios of b/a type transitions are listed in the table. The latter values were calculated from directions of transition dipole moments relative to principal axes of rotation. In most cases magnitudes of transition moments become larger by substitution, in particular at the 1-position. Directions of transition moments relative to principal axes of rotation are different from molecule to molecule. However, this is due to changes in the relative angles of principal axes of rotation and transition moment vectors are almost parallel to the C═O bond and slightly tilted to the terminal carbon atom in all radical species. An intensity ratio of the b-type to a-type transition was calculated to be 0.442 for CH_2CHO. This value is very close to the value of 0.4 reported by Brock et al.[8] rather than those by DiMauro et al.[5] and Nagai et al.[9] who estimated smaller contribution of the b-type transition. In the case of CH_2CFO, Wright et al. estimated this ratio as 0.577,[17] which is also in good agreement with the calculated value of 0.596.

Radiative lifetimes of the 0−0 bands of vinoxy type radicals were calculated as inverse of Einstein's *A*-coefficients by using calculated transition moments and experimental transition energies of the 0−0 bands. Experimentally observed fluorescence lifetimes of the 0−0 bands were plotted against calculated radiative lifetimes, and the points show an almost linear relationship (Figure 4), indicating the fluorescence lifetimes of the 0−0 band are determined by radiative lifetimes.

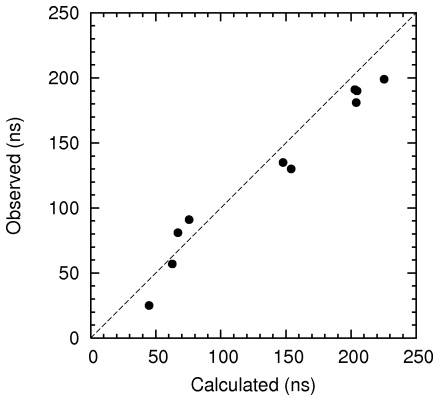

Figure 4. Observed fluorescence lifetimes of vibrationless level of the $\tilde{B}$ state plotted against calculated fluorescence lifetimes.

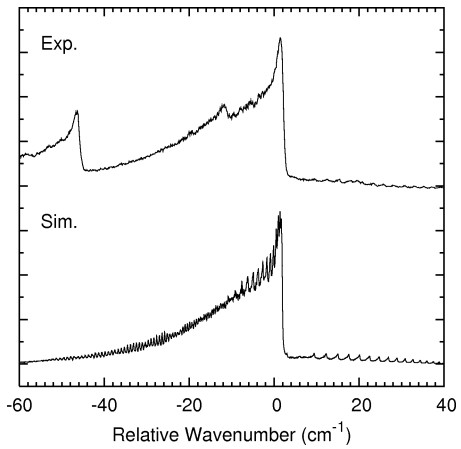

Figure 5. Rotational profiles of the 0−0 band of *trans*-CHClCHO radical: (upper) measured at room temperature; (lower) simulated at 300 K.

Simulation of Rotational Profiles of Chlorinated Vinoxy Radicals. Although rotational constants have been experimentally determined for CH_2CHO and CH_2CFO radicals as described above, rotational constants of other radicals have not been determined experimentally. LIF measurements were performed at room temperature and only broad rotational profiles have been observed. On the basis of the successful calculation of transition moments at MRCISD level, we performed simulations of rotational profiles in fluorescence excitation spectra of chlorinated vinoxy radicals by using calculated rotational constants and directions of transition moments.

Rotational constants at planar optimized geometries in $\tilde{X}$ and $\tilde{B}$ states were used for simulation. Molecules were assumed as asymmetric rotors and neither centrifugal distortion nor spin−rotation interaction was taken into account. Figure 5 shows rotational profiles of the 0−0 band of *trans*-CHClCHO radical in the fluorescence excitation spectrum after the reaction of CH_2CCl_2 + $O(^3P)$ at room temperature.[19] The spectrum of *trans*-CHClCHO shows that the 0−0 band at 29040 cm^{-1} and hot bands at 28993, 28947, and 28898 cm^{-1} have a tail on the lower wavenumber side. A simulated spectrum of the 0−0 band of *trans*-CHClCHO in Figure 5 shows an asymmetrical peak with a tail on the lower wavenumber side and its width at half height was about 60 cm^{-1}. It is noteworthy that the simulated band profile shows very good agreement with the measured band profile without adjusting the input parameters.

Figure 6 shows rotational profiles of the 0−0 band of *cis*-CHClCHO. The 0−0 band of *cis*-CHClCHO appears at 28412 cm^{-1} accompanying a slightly smaller peak at 28423 cm^{-1} and a bunch of small sharp peaks extending to the lower wavenum-

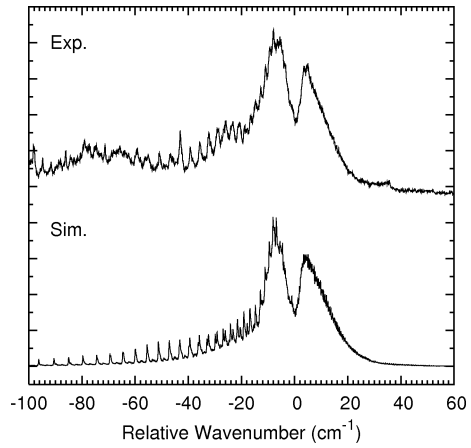

Figure 6. Rotational profiles of the 0−0 band of *cis*-CHClCHO radical: (upper) measured at room temperature; (lower) simulated at 300K.

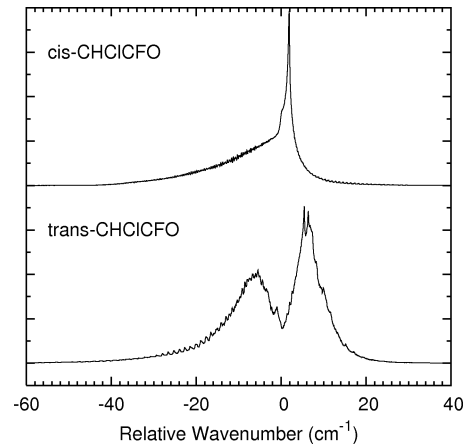

Figure 7. Simulated rotational profiles of the 0−0 bands of CHClCFO radicals at 300 K: (upper) *cis*-CHClCFO; (lower) *trans*-CHClCFO.

ber side. The simulated spectrum of *cis*-CHClCHO shows two peaks separated by 11 cm^{-1} and the peak at the higher wavenumber side is slightly smaller. On the lower wavenumber side of these two intense peaks, small sharp peaks arise from ^rR_n transitions. These features are in good agreement with the observed rotational profile of the 0−0 band of this radical. The band origin was adjusted to 28418.5 cm^{-1} in the simulation. Rotational constants in the $\tilde{B}$ state were slightly modified to 0.5246, 0.1327, and 0.1059 cm^{-1} from the values at the planar optimized geometry as listed in Table 5 by adjusting CCO and CCCl angles 2° smaller. Although it cannot be confirmed this adjustment is a unique solution to reproduce the observed profile, it is probable that calculated CCO and CCl bond angles are less accurate than other geometrical parameters due to nonbonding interaction between oxygen and chlorine atoms in *cis*-conformer, which would be difficult to describe by using the basis sets employed for the present calculation.

Figure 7 shows simulated spectra of *trans*- and *cis*-CHClCFO radicals. The spectrum of *cis*-CHClCFO shows a single sharp peak with a tail extending to the lower wavenumber, which is in good agreement with the profile of the 0−0 band of the radical at 30715 cm^{-1} in the fluorescence excitation spectrum.[20] On the other hand, the simulated spectrum of *trans*-CHClCFO shows sharp peaks at 2 and 5 cm^{-1}, and there is a broad peak at −8 cm^{-1}. Inomata et al. have found a small peak at 30066 cm^{-1} in the excitation spectrum of $CHCl{=}CF_2 + O$ whose profile is different from that of *cis*-CHClCFO. The observed profile of the peak at 30066 cm^{-1} is very similar to the simulated profile of *trans*-CHClCFO. As listed in Table 6, the calculated T_0 value of *trans*-CHClCFO is 30669 cm^{-1}, which is in good agreement with the observed value of 30066 cm^{-1}, and we tentatively assign the peak at 30066 cm^{-1} as *trans*-CHClCFO.

Threshold of Fast Nonradiative Decay. The fluorescence excitation spectrum of vinoxy radical disappears at 1300 cm^{-1} above the 0−0 band, although vibronic levels above this threshold have been confirmed by several different methods, indicating that a very fast nonradiative decay pathway becomes accessible.[6,10] One of the authors pointed out that the threshold might correspond to a barrier on the potential energy curve of $\tilde{B}$ state along the C−C rotation and the very fast decay to the lower states occur at C−C twisted geometry as the energy of $\tilde{A}$ state becomes very close to that of $\tilde{B}$ state.[13] Matsika et al. performed a thorough study on this predissociation mechanism, and the nonradiative decay from $\tilde{B}$ state to $\tilde{A}$ state does not proceed through conical intersections but is mediated by nonadiabatic coupling between $\tilde{B}$ and $\tilde{A}$ states.[14] They performed a model calculation of nonradiative decay rates from vibronic levels on the $\tilde{B}$ state by using one-dimensional potential energy curves. Decay rates increased significantly above vibronic levels in which vibrational wave functions are delocalized to nonplanar structure where the nonadiabatic coupling constant is very large. Recently, Bacchus-Montabonel et al. calculated adiabatic potential surfaces and nonadiabatic coupling constants of vinoxy radical in the ground and excited states and identified the location where nonadiabatic coupling between $\tilde{B}$ and $\tilde{A}$ states becomes significant.[57]

We expected that the proposed mechanism of the fast nonradiative decay from the $\tilde{B}$ state is basically common for all the vinoxy type radicals. Thus we calculated energy differences between planar and nonplanar optimized geometries to see whether there is any correlation between the energy differences and observed thresholds of fast nonradiative decay.

Table 8 shows optimized geometries at stationary points on the $\tilde{B}$ state of vinoxy radical. Two local minima at nonplanar optimized geometries (LMB1 and LMB2) were found and saddle points (SPB1 and SPB2) from the planar optimized geometry at the spectroscopic minimum (SMB) to LMB1 and LMB2 geometries were also located. The central CH bond is parallel (LMB1) or perpendicular (LMB2) to the plane of the terminal CH_2, and the former has much lower total energy than the latter. Although the optimized geometry of LMB1 is very close to that already reported by Matsika et al., LMB2 has not been reported. The CCO bond angle decreases as SMB > SPB > LMB along the paths. This decrease of the CCO bond angle is similar to the case of the allyl radical, which shows conrotatory and disrotatory pathways to ring closure with concomitant decrease of the CCC bond angle, although in the case of vinoxy the reaction pathway from the $\tilde{B}$ state is not directly connected to the ground state of a cyclic product.

Table 9 shows energy differences between planar and nonplanar optimized geometries. In the case of CH_2CXO radicals, energy differences between LMB1 and SMB are larger than that of CH_2CHO in all cases. This result is consistent with the observation on CH_2CFO and CH_2COCH_3 whose vibronic levels have been observed to 2500 and 2800 cm^{-1} above from the 0−0 band in fluorescence excitation spectra, indicating higher onset of the fast nonradiative decay than that of vinoxy. However, CH_2CClO has not been detected by laser-induced fluorescence, although the onset of the predissociation is expected to be high enough for fluorescence to be observed.

In contrast, calculated energy differences of CHXCHO radicals are smaller than that of CH_2CHO. Vibronic bands of

TABLE 8: Planar and Nonplanar Optimized Geometries of CH_2CHO

	SMX[a]	SMB[b]	SPB1[c]	LMB1[d]	SPB2[e]	LMB2[f]
total energy (hartree)	−152.7655	−152.6334	−152.6228	−152.6273	−152.6139	−152.6173
ΔE (cm^{-1})	−29008	0	2313	1326	4275	3523
$R(C_1-C_2)$	1.437	1.447	1.466	1.463	1.468	1.469
$R(C_2-O)$	1.236	1.374	1.367	1.358	1.359	1.350
$R(C_2-H_3)$	1.108	1.094	1.094	1.096	1.098	1.095
$R(C_1-H_1)$	1.089	1.088	1.091	1.093	1.094	1.091
$R(C_1-H_2)$	1.089	1.087	1.089	1.090	1.090	1.093
$\angle(C_1\text{-}C_2\text{-}O)$	122.8	122.7	109.2	101.4	116.1	108.5
$\angle(C_1\text{-}C_2\text{-}H_3)$	116.9	120.3	120.5	118.9	121.1	125.2
$\angle(C_2\text{-}C_1\text{-}H_1)$	119.1	119.9	122.3	122.5	121.0	120.7
$\angle(C_2\text{-}C_1\text{-}H_2)$	121.2	119.8	118.1	118.2	120.6	120.0
$\angle(H_3\text{-}C_2\text{-}C_1\text{-}O)$	180.0	180.0	141.3	128.7	141.7	145.7
$\angle(H_1\text{-}C_1\text{-}C_2\text{-}O)$	180.0	180.0	−129.2	−117.7	−75.0	113.1
$\angle(H_2\text{-}C_1\text{-}C_2\text{-}O)$	0.0	0.0	39.9	50.2	98.5	−53.8

[a] Planar optimized geometry in the $\tilde{X}$ state. [b] Planar optimized geometry in the $\tilde{B}$ state. [c] Saddle point between SMB and LMB1. [d] Nonplanar optimized geometry 1 in the $\tilde{B}$ state. [e] Saddle point between SMB and LMB2. [f] Nonplanar optimized geometry 2 in the $\tilde{B}$ state.

TABLE 9: Energy Differences between Planar (SMB) and Nonplanar (LMB) Optimized Geometries in the $\tilde{B}$ State and Thresholds of Fast Nonradiative Decay Observed in the Fluorescence Excitation Spectra

	torsion angle[a] (deg)	ΔE (cm^{-1})	threshold (cm^{-1})
CH_2CHO	−118.8	1326	1190[b]
CH_2CFO	−129.6	3830	>2700[c]
CH_2CClO	−123.9	3275	not observed[d]
CH_2COCH_3	115.8	2410	2800[e]
trans-CHClCHO	−118.1	634	1550[d]
trans-CH_3CHCHO	−103.6	759	900[f]

[a] Defined as 1/2 ($\angle(H_1-C_1-C_2-O) + \angle(H_2-C_1-C_2-O) + \angle(H_1-C_1-C_2-H_3) + \angle(H_2-C_1-C_2-H_3)$). [b] Reference 8. [c] Reference 18. [d] Reference 19. [e] Reference 23. [f] Reference 24.

trans-CHClCHO were observed up to 1550 cm^{-1} higher from the 0−0 band, which is higher than the threshold of fast decay of vinoxy determined by Brock et al. However, they report that the fluorescence lifetime of the band at 1567 cm^{-1} above the 0−0 band of vinoxy was 14 ns and more vibronic bands are detected in the higher wavenumber region with their fluorescence lifetimes less than 1 ns. Therefore, the smaller calculated energy difference in the case of *trans*-CHClCHO is not necessarily inconsistent with the observation if thresholds of the nonradiative decay of both radicals were determined on the basis of fluorescence lifetimes of vibronic bands.

In the case of 2-methylvinoxy, fluorescence excitation spectrum showed vibronic bands of both *trans*- and *cis*-CH_3-CHCHO. No vibronic bands were observed outside the region 29090−30260 cm^{-1} except a very weak band at 30385 cm^{-1}. Vibronic bands below 29600 cm^{-1} showed intervals and intensities characteristic of torsion of the methyl group, and they were assigned to trans and cis isomers with the lowest vibronic bands at 29363 and 29090 cm^{-1}, respectively. However, vibronic bands above 29800 cm^{-1} do not accompany such torsional patterns and they are left unassigned. If the band at 30260 cm^{-1} is assigned to *trans*-CH_3CHCHO, the threshold of fast nonradiative decay is estimated to be around 900 cm^{-1}. This experimental value of the threshold is lower than that of vinoxy and consistent with the calculated value.

As noted above, fluorescence of CH_2CClO has not been detected yet even though the calculated total energies of LMB and SMB predict the radical to be fluorescent. It is difficult to assume that CH_2CClO is not generated by reactions such as $CH_2CCl_2 + O(^3P)$ or $CH_3CClO + Cl$ on the basis of the formation of CH_2CFO from the same type of reactions. We suppose that CH_2CClO is not fluorescent even at the vibrationless level of the $\tilde{B}$ state due to a very fast nonradiative decay mechanism that is different from the one effective above the onset by nonadiabatic coupling to the lower states at nonplanar geometries. Hoops et al. mentioned that though the photofragment yield spectrum of CH_2CHO showed a distinct increase above the onset of the nonradiative decay, the photofragment yield spectrum of CH_2CFO did not show such an increase and the yield at lower vibronic levels is much higher than that of CH_2CHO. This may be due to another nonradiative decay mechanism operative at lower vibronic levels in CH_2CFO, which is further accelerated in the case of CH_2CClO by substitution to the heavier halogen atom and resulted in suppression of fluorescence of the radical. We expect that vibronic spectra of the CH_2CClO radical can be detected by measurements suitable for electronic transitions of nonfluorescent molecules.

Conclusion

We have calculated the electronic structure of vinoxy type radicals by using the MRCISD method to describe not only the ground but also the electronically excited states with sufficient accuracy. Quantitatively accurate optimized geometries, vibrational frequencies, electronic transition energies and transition moments were obtained by MRCISD calculation and these values were successfully applied for rotational analysis of vibronic spectra. In particular, excitation energies with Davidson's correction (MRCISD+Q) showed far better agreement with the observed values compared to results from the CASSCF calculation, indicating that incorporation of dynamical correlation by the MRCISD method was crucial for accurate calculation of transition energies even in the case of vinoxy type radicals, in which case CASSCF level calculation can be sufficient for description of valence excited states.

We have shown that calculated radiative lifetimes of the 0−0 bands of the radicals are in good agreement with observed values in most cases. This result means not only transition energies but also magnitudes of transition moments were calculated with sufficient accuracy. Therefore, observed lifetimes shorter than calculated values indicate the existence of fast nonradiative pathway.

Vinoxy type radicals show fluorescence excitation spectra with thresholds above which fluorescence decay rates are very large. Measured fluorescence spectra show that thresholds move to higher wavenumber upon substitution at the 1-position, whereas substitution at the 2-position shifted thresholds to lower wavenumber. These trends correspond to energy differences between planar and nonplanar local energy minima in state, as

expected from the nonradiative decay mechanism via nonadiabatic coupling to the lower states at nonplanar geometries.

These results indicate that MRCISD calculation is quantitatively accurate and helps to assign new vinoxy type radicals in measured vibronic spectra by providing the position of the 0−0 bands, rotational profiles, radiative lifetimes, Franck−Condon factors, and upper limit of the vibronic bands in the excitation spectra. In forthcoming papers we will show examples of such successful application of MRCISD calculations that support detection of novel vinoxy type radicals.

Acknowledgment. M.Y. thanks Prof. Hans Lischka for kind arrangement to give him an opportunity to use the latest version of the COLUMBUS program and gave him helpful comments and suggestions for running the program.

Supporting Information Available: Optimized geometries of vinoxy type radicals (Table S1 to S12). This material is available free of charge via the Internet at http://pubs.acs.org.

References and Notes

(1) Cvetanoviæ, R. J.; Singleton, D. L. *Rev. Chem. Int*. **1984**, *5*, 183.
(2) Ramsay, D. A. *J. Chem. Phys.* **1965**, *43*, S18.
(3) Hunziker, H. E.; Kneppe, H.; Wendt, H. R. *J. Photochem. Photobiol. A* **1981**, *17*, 377.
(4) Inoue, G.; Akimoto, H. *J. Chem. Phys.* **1981**, *74*, 425.
(5) DiMauro, L. F.; Heaven, M.; Miller, T. A. *J. Chem. Phys.* **1984**, *81*, 2339.
(6) Gejo, T.; Takayanagi, M.; Kono, T.; Hanazaki, I. *Chem. Lett.* **1993**, 2065.
(7) Wan, R.; Chen, X.; Wu, F.; Weiner, B. R. *Chem. Phys. Lett.* **1996**, *260*, 539.
(8) Brock, L. R.; Rohlfing, E. A. *J. Chem. Phys.* **1997**, *106*, 10048.
(9) Nagai, H.; Carter, R. T.; Huber, J. R. *Chem. Phys. Lett.* **2000**, *331*, 425.
(10) Osborn, D. L.; Choi, H.; Mordaunt, D. H.; Bise, R. T.; Neumark, D. M.; Rohlfing, C. M. *J. Chem. Phys.* **1997**, *106*, 3049.
(11) Dupuis, M.; Wendoloski, J. J.; Lester, W. A., Jr. *J. Chem. Phys.* **1982**, *76*, 488.
(12) Yamaguchi, M.; Momose, T.; Shida, T. *J. Chem. Phys.* **1990**, *93*, 4211.
(13) Yamaguchi, M. *Chem. Phys. Lett.* **1994**, *221*, 531.
(14) Matsika, S.; Yarkony, D. R. *J. Chem. Phys.* **2002**, *117*, 7198.
(15) Furubayashi, M.; Bridier, I.; Inomata, S.; Washida, N.; Yamashita, K. *J. Chem. Phys.* **1997**, *106*, 6302.
(16) Washida, N.; Furubayashi, M.; Imamura, T.; Bridier, I.; Miyoshi, A. *J. Chem. Phys.* **1997**, *107*, 6998.
(17) Wright, S. A.; Dagdigian, P. J. *J. Chem. Phys.* **1997**, *107*, 9755.
(18) Inomata, S.; Furubayashi, M.; Imamura, T.; Washida, N.; Yamaguchi, M. *J. Chem. Phys.* **1999**, *111*, 6356.
(19) Inomata, S.; Bridier, I.; Furubayashi, M.; Imamura, T.; Inoue, G.; Yamaguchi, M.; Washida, N. *J. Phys. Chem. A* **2001**, *105*, 7559.
(20) Inomata, S.; Yamaguchi, M.; Washida, N. *J. Chem. Phys.* **2002**, *116*, 6961.
(21) Williams, S.; Zingher, E.; Weisshaar, J. C. *J. Phys. Chem. A* **1998**, *102*, 2297.
(22) Washida, N.; Inomata, S.; Furubayashi, M. *J. Phys. Chem. A* **1998**, *102*, 7924.
(23) Williams, S.; Harding, L. B.; Stanton, J. F.; Weisshaar, J. C. *J. Phys. Chem. A* **2000**, *104*, 10131.
(24) Williams, S.; Harding, L. B.; Stanton, J. F.; Weisshaar, J. C. *J. Phys. Chem. A* **2000**, *104*, 9906.
(25) Hoops, A. A.; Gascooke, J. R.; Kautzman, K. E.; Faulhaber, A. E.; Neumark, D. M. *J. Chem. Phys.* **2004**, *120*, 8494.
(26) Yamaguchi, M.; Furubayashi, M.; Inomata, S.; Washida, N. *Chem. Phys. Lett.* **1998**, *298*, 93.
(27) Lischka, H.; Shepard, R.; Brown, F. B.; Shavitt, I. *Int. J. Quantum Chem., Quantum Chem. Symp.* **1981**, *15*, 91.
(28) Shepard, R.; Shavitt, I.; Pitzer, R. M.; Comeau, D. C.; Pepper, M.; Lischka, H.; Szalay, P. G.; Ahlrichs, R.; Brown, F. B.; Zhao J. *Int. J. Quantum Chem., Quantum Chem. Symp.* **1988**, *22*, 149.
(29) Lischka, H.; Shepard, R.; Pitzer, R. M.; Shavitt, I.; Dallos, M.; Müller, Th.; Szalay, P. G.: Seth, M.; Kedziora, G. S.; Yabushita S.; Zhang, Z. *Phys. Chem. Chem. Phys.* **2001**, *3*, 664.
(30) Lischka, H.; Shepard, R.; Shavitt, I.; Pitzer, R. M.; Dallos, M.; Müller, Th.; Szalay, P. G.; Brown, F. B.; Ahlrichs, R.; Böhm, H. J.; Chang, A.; Comeau, D. C.; Gdanitz, R.; Dachsel, H.; Ehrhardt, C.; Ernzerhof, M.; Höchtl, P.; Irle, S.; Kedziora, G.; Kovar, T.; Parasuk, V.; Pepper, J. M.; Scharf, P.; Schiffer, H.; Schindler, M.; Schüler, M.; Seth, M.; Stahlberg, E. A.; Zhao, J.-G.; Yabushita, S.; Zhang, Z. COLUMBUS, an ab initio electronic structure program, release 5.9, 2004.
(31) Shepard, R. *Int. J. Quantum Chem.* **1987**, *31*, 33.
(32) Shepard, R.; Lischka, H.; Szalay, P. G.; Kovar, T.; Ernzerhof, M. *J. Chem. Phys.* **1992**, *96*, 2085.
(33) Sheperd, R. In *Modern Electronic Structure Theory Part I*; Yarkony, D. R., Ed.; World Scientific: Singapore, 1995; p 345.
(34) Lischka, H.; Dallos, M.; Sheperd, R. *Mol. Phys.* **2002**, *100*, 1647.
(35) Dallos, M.; Müller, Th.; Lischka, H.; Sheperd, R. *J. Chem. Phys.* **2001**, *114*, 748.
(36) Müller, Th.; Lischka, H. *Theor. Chem. Acc.* **2001**, *106*, 369.
(37) Dunning, T. H., Jr. *J. Chem. Phys.* **1989**, *90*, 1007.
(38) Woon, E. E.; Dunning, T. H., Jr. *J. Chem. Phys.* **1993**, *98*, 1358.
(39) Császár, P.; Pulay, P. *J. Mol. Struct.* **1984**, *114*, 31.
(40) Fogarasi, G.; Zhou, X.; Taylor, P. W.; Pulay, P. *J. Am. Chem. Soc.* **1992**, *114*, 8191.
(41) Pulay, P.; Fogarasi, G.; Pongor, G.; Boggs, J. E.; Vargha, A. *J. Am. Chem. Soc.* **1983**, *105*, 7037.
(42) Langhoff, S. R.; Davidson, E. R. *Int. J. Quantum Chem.* **1974**, *8*, 61.
(43) Bruna, P. J.; Peyerimhoff, S. D.; Buenker, R. J. *Chem. Phys. Lett.* **1981**, *72*, 278.
(44) Frisch, M. J.; Trucks, G. W.; Schlegel, H. B.; Scuseria, G. E.; Robb, M. A.; Cheeseman, J. R.; Montgomery, J. A., Jr.; Vreven, T.; Kudin, K. N.; Burant, J. C.; Millam, J. M.; Iyengar, S. S.; Tomasi, J.; Barone, V.; Mennucci, B.; Cossi, M.; Scalmani, G.; Rega, N.; Petersson, G. A.; Nakatsuji, H.; Hada, M.; Ehara, M.; Toyota, K.; Fukuda, R.; Hasegawa, J.; Ishida, M.; Nakajima, T.; Honda, Y.; Kitao, O.; Nakai, H.; Klene, M.; Li, X.; Knox, J. E.; Hratchian, H. P.; Cross, J. B.; Bakken, V.; Adamo, C.; Jaramillo, J.; Gomperts, R.; Stratmann, R. E.; Yazyev, O.; Austin, A. J.; Cammi, R.; Pomelli, C.; Ochterski, J. W.; Ayala, P. Y.; Morokuma, K.; Voth, G. A.; Salvador, P.; Dannenberg, J. J.; Zakrzewski, V. G.; Dapprich, S.; Daniels, A. D.; Strain, M. C.; Farkas, O.; Malick, D. K.; Rabuck, A. D.; Raghavachari, K.; Foresman, J. B.; Ortiz, J. V.; Cui, Q.; Baboul, A. G.; Clifford, S.; Cioslowski, J.; Stefanov, B. B.; Liu, G.; Liashenko, A.; Piskorz, P.; Komaromi, I.; Martin, R. L.; Fox, D. J.; Keith, T.; Al-Laham, M. A.; Peng, C. Y.; Nanayakkara, A.; Challacombe, M.; Gill, P. M. W.; Johnson, B.; Chen, W.; Wong, M. W.; Gonzalez, C.; Pople, J. A. *Gaussian 03*, revision C.02; Gaussian, Inc.: Wallingford, CT, 2004.
(45) Ditchfield, R.; Hehre, W. J.; Pople, J. A. *J. Chem. Phys.* **1971**, *54*, 724.
(46) Hehre, W. J.; Ditchfield, R.; Pople, J. A. *J. Chem. Phys.* **1972**, *56*, 2257.
(47) Francl, M. M.; Pietro, W. J.; Hehre, W. J.; Binkley, J. S.; Gordon, M. S.; DeFrees, D. J.; Pople, J. A. *J. Chem. Phys.* **1982**, *77*, 3654.
(48) Hariharan P. C.; Pople, J. A. *Theor. Chim. Acta* **1973**, *28*, 213.
(49) *SpecView*: Simulation and Fitting Of Rotational Structure Of Electronic And Vibronic Bands. V. L. Stakhursky, T. A. Miller, 56th Molecular Spectroscopy Symposium. http://www.chemistry.ohio-state.edu/~vstakhur.
(50) Botschwina, P. *Mol. Phys.* **2005**, *103*, 1441.
(51) Endo, Y.; Saito, S.; Hirota, E. *J. Chem. Phys.* **1985**, *83*, 2026.
(52) Endo, Y.; Hirota, E. *J Mol. Spectrosc.* **1988**, *127*, 535.
(53) Cao, D.; Ding, Y.; Li, Z.: Huang, X.: Sun, C. *J. Phys. Chem. A* **2002**, *106*, 8917.
(54) Scott, A. P.; Radom, L. *J. Phys. Chem.* **1996**, *100*, 16502.
(55) Utkin, Y. G.; Han, J.-X.; Sun, F.; Chen, H.-B.; Scott, G.; Curl, R. F. *J. Chem. Phys.* **2003**, *118*, 10470.
(56) NIST Computational Chemistry Comparison and Benchmark Database, NIST Standard Reference Database Number 101, Release 12, Aug 2005; Johnson, Russell D., III, Ed.; http://srdata.nist.gov/cccbdb.
(57) Bacchus-Montabonel, M. C.; Piechowska, K.; Tergimana, Y. S.; Sienkiewicz, J. E. *J. Mol. Struct. (THEOCHEM)* **2005**, *729*, 115. Piechowska-Strumik, K.; Bacchus-Montabonel, M.-C.; Tergiman Y. S.; Sienkiewicz, J. E. *Chem. Phys. Lett*. **2006**, *425*, 225.